Advances in Hydrogen Energy Technologies:
Oportunities and Challenges in a Hydrogen Economy
4th International Seminar - November 10-11, 2011, Viana do Castelo - Portugal

Relaxation time distribution analysis of a polymer electrolyte fuel cell stack from its impedance response

Vitor V. Lopes[1], R. A. Silva[2], Augusto Q. Novais[1], C. M. Rangel[2]

[1]Energy Systems Modeling and Optimization Unit, LNEG, National Laboratory for Energy and Geology,
Estrada do Paço do Lumiar, 22, 1649-038 Lisboa, Portugal
email: vitor.lopes@lneg.pt
[2]Fuel Cells and Hydrogen Unit, LNEG, National Laboratory for Energy and Geology,
Estrada do Paço do Lumiar, 22, 1649-038 Lisboa, Portugal
email: carmen.rangel@lneg.pt

Abstract

Electrochemical impedance spectroscopy (EIS) is an analysis technique that is commonly used as a base diagnostics technique for the in-situ analysis of the kinetic and transport properties of proton exchange membrane (PEM) fuel cells. This work proposes to use the distribution of relaxation times (DRT) as a complementary analysis technique for the interpretation of EIS data. For this purpose, the DRT is deduced for a modified Randles electric circuit composed of a constant phase element (CPE) connected in parallel with a resistance in series with a finite diffusion Warburg element. The experimental EIS data collected from an eight cell PEMFC with an open-air cathode was modeled through the use of two modified Randles circuit representing the fuel-cell electrodes. The analysis of the DRT allows to identify further characteristics of the individual processes that occur at both electrodes, while also being instrumental in detecting the effect on the fuel cell performance of some operating conditions, namely hydrogen flow-rate and current.

Keywords: *Distribution of relaxation times, Electrochemical impedance spectroscopy, Proton exchange membrane fuel cell*

1 Introduction

The urge for highly efficient and environmental friendly technologies addressing energy generation systems has been a major driving force for the research in fuel cells. Specifically, hydrogen polymer electrolyte fuel cells (PEMFC) are a strong alternative for the development of portable applications since they can achieve high energy densities [1].

The fuel cell stack performance is highly dependent on the different electrochemical, but also physical phenomena occurring inside the cells. For instance, water excess may cause liquid to block the gas transport in the electrodes, gas diffusion layers and cell gas channels; water deficiency, on the other hand, due to cell membranes drying out under high voltage and temperature conditions, may lead to a decrease in their protonic conductivity [2].

For the diagnosis and the characterization of these phenomena, electrochemical techniques such as polarization curves and EIS [3], are commonly employed.

Polarization curves allow to characterize the PEMFC steady-state current-voltage response and extract information about the effects of the different operating conditions (such as composition or flow rates) upon the performance of the system [4]; EIS can capture the transient response of the system and thus allows the identification of the phenomena associated with membrane conductivity, kinetic and mass transport limitations by taking advantage of their different time scales [5]. The strategy to model EIS generally requires, first to formulate an equivalent electric circuit model to describe the experimental data, and then to estimate the model parameters by using a complex nonlinear least squares regression (CNLS) technique [6]. One of the main drawbacks in the use of electric circuits to explain EIS is its non-uniqueness, i.e. the same EIS behaviour can be represented by very distinct circuits.

To address this issue, the article proposes to use of the distribution of the relaxation times (DRT) as a complementary analysis technique for interpreting EIS data. When a system is linear and non-resonant, its frequency response may be related to a DRT. It is used when the observed impedance data cannot be explained in terms of a Debye process involving not one single relaxation time, but rather

an entire line spectrum or continuous spectrum of relaxation times [7]. Herein this technique is applied to the characterization of the factors affecting the performance of the fuel cells and an analysis is presented of EIS data obtained from a fuel-cell stack under different operating conditions. A two-step methodology is proposed and the results are analysed in terms of the different mass-transfer diffusion regimes occurring inside the fuel-cell.

2 Experimental

An eight-cell stack, with an active area of 3.8 cm2, was employed, using a commercial catalyst coating membrane (3M) and GDL (gas diffusion layer, Johnson Matthey). Bipolar plates were made of graphite from Schunk, with anode flow fields having a proprietary design. The stack has an open-cathode with vertical channels. An air fan is located at the edge of the manifolds providing high stoichiometry oxidant supply and stack cooling. A purpose-built fuel cell testing station was used to control the inlet temperature, pressure and flow rate for the anode gas stream. Impedance measurements were carried out using a Solartron Frequency Response Analyser Model 1260. The frequency was typically spanned between 20 kHz and 0.1 Hz. The EIS dataset was collected under a fixed air flow-rate (8.0 $Lmin^{-1}$) and hydrogen pressure (0.5bar) by changing the hydrogen flow-rate (0.2, 0.4, 0.6 $Lmin^{-1}$) and the current (0.35A, 0.5A, 1.0A, 1.5A).

3 Methodology for the computation of the distribution of relaxation times from EIS data

The methodology for the analysis of EIS data is based on a two step procedure: first, a mathematical impedance model is fitted to the experimental data and afterwards the DRT function is derived using the methodology presented in Fuoss and Kirkwood [8].

3.1 PEM fuel cell impedance modeling

EIS data can be modeled by using the concept of equivalent electrical circuit. For this work, the impedance model is represented by the combination of a resistance with two modified Randles electric circuits [9] (Figure 1).
The model is composed of three main components: a pure resistance element commonly associated with the PEM fuel-cell membrane contribution plus those for the anode and cathode. The dynamic behaviour of each electrode is represented by the modified Randles circuit which is composed of a constant-phase element (CPE) in parallel with a resistance in series with a finite diffusion Warburg element. This model is capable to account for different mass diffusion transport effects and non-ideal polarized electrodes. It may be expressed mathematically through the following equation:

$$Z(w) = R_0 + \frac{1}{C_a(jw)^{\alpha_a} + \frac{1}{R_a + Z_{D,a}(w)}} + \frac{1}{C_c(jw)^{\alpha_c} + \frac{1}{R_c + Z_{D,c}(w)}} \quad (1)$$

where w is the frequency (Hz), j is the imaginary unit, C_a and C_c are the anodic and cathodic CPE constants, α_a and α_c are the CPE exponents which range from 1 (a pure condenser) to 0 (a pure resistance), passing by the infinite diffusion Warburg-like behavior when reaching ½; R0, Ra and Rc are, respectively, membrane, anodic and cathodic resistances; and, $Z_{D,a}(w)$ and $Z_{D,c}(w)$ are the anodic and cathodic finite Warburg diffusional elements given by:

$$Z_{D,i}(w) = R_{D,i} \frac{\tanh\sqrt{jw\tau_{D,i}}}{\sqrt{jw\tau_{D,i}}} \quad (2)$$

in which $\tau_{D,i}$ is related to the mass transfer time constants and $R_{D,i}$ is the associated anodic and cathodic finite diffusional Warburg resistance.

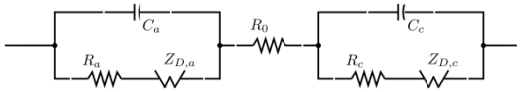

Fig. 1. Equivalent electric circuit composed by a resistance in series with two modified Randles circuits used for PEM fuel cells characterization by EIS.

3.2 Identification of the model parameters

The main goal in the system identification is to estimate the (real valued) model parameters:
$\theta = [R_0, R_a, C_a, R_{D,a}, \tau_{D,a}, \alpha_a, R_c, C_c, R_{D,c}, \tau_{D,c}, \alpha_c]$
for the model defined by Eq. 1, from a discrete set of measured frequency response data $Z_m(w_n)$, with $n = 1 \ldots N$. The parameters are identified by solving the complex nonlinear least squares (CNLS) minimization problem, defined by the following quadratic objective function:

$$\mathrm{FO}(\theta) = \frac{1}{2}\sum_{n=1}^{N} \varepsilon_n(\theta)^{\mathrm{H}}\, \varepsilon_n(\theta) \quad (3)$$

where

$$\varepsilon_n(\theta) = Z_m(w_n) - Z(w_n, \theta) \quad (4)$$

i.e. $\varepsilon_n(\theta)$ is the difference between the measured frequency response data $Z_m(w_n)$ and the model estimates $Z(w_n, \theta)$; w_n is the frequency value, N the number of data points and $\varepsilon_n(\theta)^{\mathrm{H}}$ the complex conjugate transpose of $\varepsilon_n(\theta)$.

The non-convexity associated with the EIS models prevents the direct estimation of the model parameters. The Levenberg-Marquardt (LM) method [10] is commonly used in this kind of optimization problems though it does not always warrant good estimates for the model parameters. In particular, the existence of multiple minima due to the non-convexity of $FO(\theta)$ and the possibility of outliers in the experimental data-set increases the risk of poor parameter estimates by the direct application of the method.

To minimize this risk, an optimization strategy based on the combination of the random sample consensus algorithm (RANSAC) with the LM method is used [11]. Figure 2 presents the strategy outline. It starts by randomly picking a subset of the data (step 1), with cardinality equal to the number of parameters, which meets the condition of being as small as possible to minimize the risk of selecting outliers, but high enough to allow the solution of the LM inner linear system.

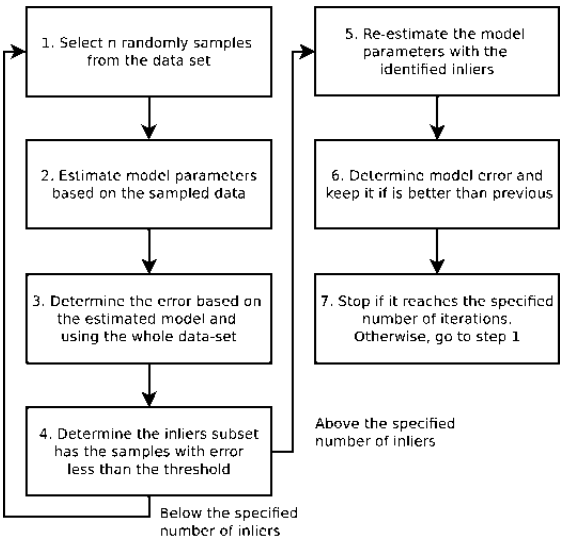

Fig. 2. Schematic of the applied optimization strategy Modified random sampling consensus algorithm to the convergence performance of the Levenberg-Marquardt method.

In step (2), the model parameters are estimated by using the LM method with the parameters initiated randomly. Then, the errors are evaluated based on the estimated parameters and using the whole data-set (step 3), followed by the determination of which samples are inliers by selecting those with an error smaller than a given threshold (step 4). This threshold is computed by using a robust statistic estimator for the error variance, based on the errors determined with the parameters computed in step 3. If the number of inliers is less than $0.75N$ then a return is made to step 1. Otherwise the model parameters are re-estimated using the LM method with the inliers subset (step 5). If the value of the objective function $FO(\theta)$ is lower than the previously known value, then the consensus subset is updated and the model parameters kept (step 6). Iteration proceeds until a stop criterion is reached.

3.3 Distribution of relaxation times for the modified Randles electric circuit

The frequency response of a linear and non-resonant dynamic system can be related to a distribution of relaxation times $G(\tau)$ by using:

$$Z_i(s) = \int_0^{+\infty} \frac{G_i(\tau)}{1+s\,\tau} d\tau \qquad (5)$$

where $Z_i(s)$ is the transfer function representing the modified Randles electric circuit for a given fuel-cell electrode and $s = jw$ is a complex frequency variable. If the transfer function is not normalized ($Z_i(0) \neq 1$) then the DRT function $G_i(\tau)$ will be non-normalized with:

$$Z_i(0) = \int_0^{+\infty} G_i(\tau) d\tau = R_i + R_{D,i} \qquad (6)$$

Equation 5 can be solved analytically [12] using:

$$G_i(\tau) = -\lim_{\varepsilon \to 0^+} \frac{1}{\pi} Im\left(Z_i\left(-\frac{1}{\tau} - j\varepsilon\right)\right) \qquad (7)$$

where the Im is the imaginary part of the complex number Z_i. The final expression for $G_i(\tau)$ can be simplified to give:

$$G_i(\tau) = \frac{\tau^{\alpha_i} \sin \alpha_i \pi}{\pi C_i \left((\sin \alpha_i \pi)^2 + \left(\cos \alpha_i \pi + \frac{(\tau/\tau_{0,i})^{\alpha_i}}{1 + \frac{R_{D,i}}{R_i} \frac{\tan \sqrt{\tau_{D,i}/\tau}}{\sqrt{\tau_{D,i}/\tau}}} \right)^2 \right)} \qquad (8)$$

where $\tau_{0,i} = (C_i R_i)^{1/\alpha_i}$ is the circuit characteristic response time in the absence of the finite diffusion Warburg element. This DRT function reduces to the Cole-Cole distribution when $\tau_{D,i}$ or $R_i/R_{D,i}$ takes very small values.

4 Results and discussion

In what follows the analysis focus the effect of the supply hydrogen flow-rate and current demand on the fuel cell performance, all other operating conditions remaining constant.

4.1 The effect of the current

Figures 3 and 4 show, respectively, the EIS impedance experimental data together with the model fitting and the corresponding DRT functions.

Figure 3 shows typical Nyquist loci characteristic of a distribution of relaxation processes (depressed semicircles) dominated by the fuel cell cathode response. The ohmic resistance slightly decreases with current increase. The total resistance shows the same trend. This is an expected behaviour related with the higher production of water for higher currents which gives place to a more hydrated membrane and less total resistance, as higher currents and power are demanded from the cell. The fitted impedance models are in good agreement with the EIS experimental data, thus allowing for an accurate determination of the corresponding DRT function (Figure 4), applying the same model to the entire current range.

In the DRT diagram, location of the peaks are associated to characteristic relaxation times whilst the area of the peak is related to the process resistance. It allows the identification of two time constants with maxima separated by a decade. Peaks are observed to be symmetric with respect to the principal time constant. This reflects the negligible impact of the Warburg finite elements (Figure 1) to the correspondent DRT and, thus, their shapes become similar to the Cole-Cole distributions. For the process located at higher relaxation times (full line) there is a monotonic decrease of α from 0.91 to 0.87 (not shown) indicating a very small broadening of the DRT distribution with the current increase. For the other process, α does not show any trend and its value ranges between 0.53 and 0.56. The associated resistances decrease with increasing current while that the characteristic time shifts towards lower values, indicating faster processes. It is also found, for higher relaxation times, that the DRT curves are sharper than those at lower values, which present a much higher dispersion.

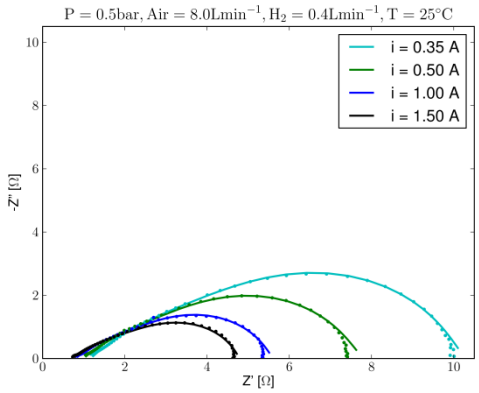

Fig. 3. Nyquist plot showing the impedance data (dots) and the model predictions (line) for the different current levels.

A first examination led us to assign the two modes, respectively, to the cathode (higher τ) and anode processes (lower τ). However, due to the high dispersion ($\alpha \cong 0.54$) of the peaks located at lower relaxation times further modeling using only one modified Randles circuit was attempted. Results suggested that both peaks could be predominantly assigned to the cathode response. Also, and in addition, that the charge transfer and mass transfer processes have been deconvoluted, with a Warburg contribution present at higher τ's.

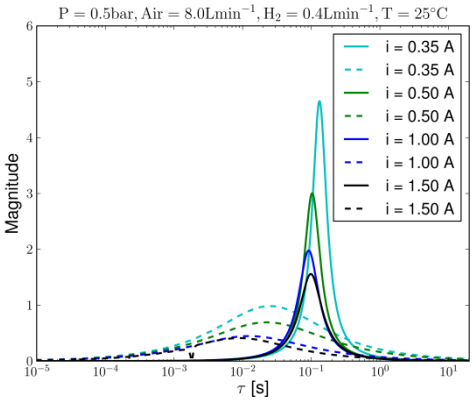

Fig. 4. DRT functions for the processes identified from the impedance data for different current levels. The two process correspond to the two terms defined in equation 1 and are coded by a dashed and full line.

4.2 The effect of the hydrogen flow-rate

This was studied in the same experimental conditions used in section 4.1. Selected results show typical responses at low (0.35A) and high (1.5A) currents. Figure 5 shows the Nyquist plot for different hydrogen flow-rates at 0.35A.

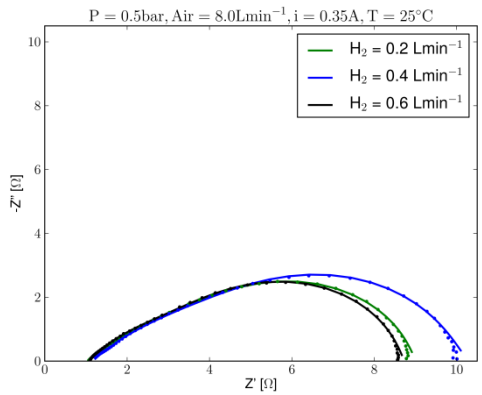

Fig. 5. Nyquist plot showing the impedance data (dots) and the model predictions (line) for different hydrogen flow-rates and $i = 0.35A$.

The change in the hydrogen flow rate affects the total resistance: taking 0.4 Lmin-1 as a basis value used to ascertain the current effect, it is found that

either an increase or a decrease in hydrogen flow rate bring about a decrease in the total resistance. However, Nyquist diagrams show poor resolution with possible overlap of individual processes. But since a good agreement between the fitted model and the experimental data is observed, these data can also be used with confidence for the determination of the respective DRT functions.

Figure 6 shows the DRT functions for the two identified processes and three different hydrogen flow-rates and low current operating conditions.
As in the previous case, it is thought that the impedance response is predominantly representative of the cathodic processes.

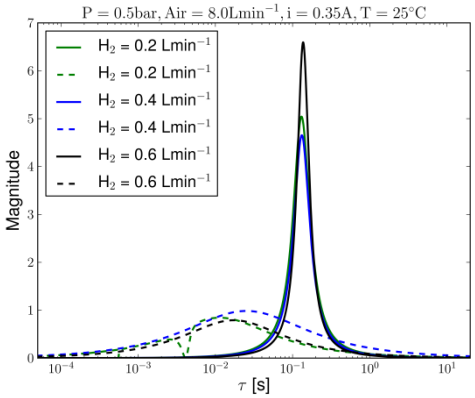

Fig. 6. DRT functions for the two processes (dashed and full line) identified from the impedance data for different hydrogen flow-rates and $i = 0.35A$.

The analysis of the higher relaxation time process (full line) shows that its DRT functions are Cole-Cole distributions, and their τ_{max} values do not change with the increase in hydrogen flow. The main change occurs in the total resistance which increases markedly for 0.6 $Lmin^{-1}$, by comparison with the remaining two flow-rates.

When the current is increased to 1.5A (Fig.7), the analysis of the DRT reveals a more clear anode effect with an increase in the hydrogen flow-rate. The figure shows the two DRT curves obtained for two different hydrogen flow-rates, 0.4 Lmin^{-1} (blue) and 0.6 Lmin^{-1} (black). For the low flow-rate there are two main processes identified, corresponding to Cole-Cole distributions centred at $\tau = 0.009s$ and $\tau = 0.098s$. To characterize the nature of these two processes, a more detailed analysis was performed by fitting the associated impedance curve to a model with a single modified Randles circuit. Results suggest that these processes were associated with the cathodic side, with the process centred at $\tau = 0.098s$ attributed to the Warburg finite diffusion element and, thus, related to mass transfer diffusion limitations.

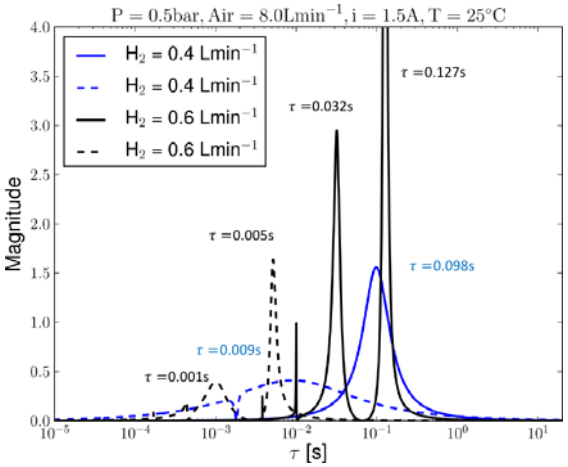

Fig. 7. DRT functions for the two processes (dashed and full line) identified from the impedance data for different hydrogen flow-rates and $i = 1.50A$.

The DRT for the high hydrogen flow-rate shows the two processes associated with the two modified Randles circuits present in the model. In this case, the contribution from the Warburg finite diffusion element is not negligible and introduces a multi-modal DRT with several coupled peaks. From the analysis of equation 8, it is possible to associate the first peak (counting from right to left) with the $\tau_{D,i}$, the Warburg finite diffusion characteristic time, and the second peak with $\tau_{0,i}$, the characteristic time of the modified Randles circuit without the Warburg element, i.e. a simple R-CPE circuit. The remaining peaks are non-dominant, i.e. their contribution to the overall DRT area is negligible and correspond to the coupling effect of the two main dominant relaxation times, $\tau_{0,i}$ and $\tau_{D,i}$.

As shown, the DRT analysis allows detecting the presence of distinct phenomena affecting the mass transfer transport, both in terms of their nature, as revealed by the observed patterns, and their location, whether on the anodic or cathodic sides of the fuel-cell.
Notwithstanding, the DRT analysis although leading to additional insight on the performance of fuel cells, can only be used to complement existing expertise, since it is not self-validating.

5 Conclusions

This paper proposes a method to derive the distribution of relaxation times from experimental impedance data. The approach is based on the fitting of a semi-empirical model for the impedance data that can account for distinct mass-transfer regimes. Based on this model the analytical

expression for the distribution of the relaxation times is derived and used to analyze different experimental impedance curves. The results show that this model is capable of describing all the analyzed cases, provided there is a good agreement between the data and the model predictions. The analysis of the DRT allows to extract information about the different nature of the mass-transfer processes, to determine their location and to identify those that more adversely affect the fuel-cell performance.

References

[1] S. Gottesfeld, T. A. Zawodzinski, Polymer Electrolyte Fuel Cells, Wiley-VCH Verlag GmbH, 2008, pp. 195–301.

[2] A. Maher, S. Al-Baghdadi, In: Fuel Cell Research Trends, Editor: L.O. Vasquez, Nova Science Publishers Inc, 2007.

[3] E. Barsoukov, J. Macdonald (Eds.), Impedance Spectroscopy Theory, Experiment, and Applications, John Wiley & Sons, 2005.

[4] V. Lopes, A. Novais, C. Rangel, Hydrogen PEMFC Stack Performance Analysis: A Data-Driven Approach, International Journal of Hydrogen Energy, 2010, 35, 18 pp: 9973-9982

[5] X. Yuan, C. Song, H., J. Zhang, Electrochemical Impedance Spectroscopy in PEM Fuel Cells Fundamentals and Applications, Springer, London, 2010.

[6] M. E. Orazem, B. Tribollet, An Integrated Approach to Electrochemical Impedance Spectroscopy, Electrochimica Acta 53 (25), 2008 pp. 7360-7366.

[7] J. MacDonald, Some Statistical Aspects of Relaxation Time Distributions, Physica, 28, 1962, 485-492.

[8] R. Fuoss and J.G.Kirkwood, Electrical Properties of Solids. VIII. Dipole Moments in Polyvinyl Chloride-Diphenyl Systems Journal of America Chemical Society, 63, 1941 pp. 385.

[9] M. Iftikhar, D. Riu, F. Druart, S. Rosini, Y. Bultel, N. Retière, Dynamic Modeling of Proton Exchange Membrane Fuel Cell Using Non-Integer Derivatives, Journal of Power Sources, 160, 2, 2006, pp. 1170-1182

[10] J. Morè, The Levenberg-Marquardt Algorithm: Implementation and Theory, in: G. Watson (Ed.), Numerical Analysis, Vol. 630 of Lecture Notes in Mathematics, Springer, Berlin/Heidelberg, 1978, pp. 105-116

[11] V. Lopes, C. Rangel, A. Novais, Fractional-Order Transfer Functions Applied To The Modeling of Hydrogen PEM Fuel Cells, In 21st European Symposium on Computer Aided Process Engineering, 2011, 29 Pages: 1748-1752

[12] J. Macdonald, Linear-System Integral Transform Relations, Reviews of Modern Physics, 28, 4, 1956, pp. 393-422